Clays and Clay Minerals, Vol. 52, No. 1, 66–84, 2004.

ILLITE-SMECTITE MIXED-LAYER MINERALS IN FELSIC VOLCANICLASTIC ROCKS FROM DRILL CORES, KAKKONDA, JAPAN

ATSUYUKI INOUE*,†, ALAIN MEUNIER AND DANIEL BEAUFORT

HydrASA-UMR 6532 CNRS, Université de Poitiers, 40 av. Recteur Pineau, 86022 Poitiers Cedex, France

Abstract—Crystallization processes of the illite-smectite (I-S) mixed-layer mineral series during alteration of felsic vitric materials in volcaniclastic sediments through two drill holes (IT-2 and IT-8) near the Kakkonda active geothermal system, Japan, were examined by optical microscopy, scanning and transmission electron microscopy (SEM and TEM), electron microprobe analysis, X-ray diffraction (XRD), and oxygen isotope analysis. Temperatures measured through the drill holes increased nearly linearly with depth up to 317ºC at the bottom (1700 m) of IT-8. Homogenization temperature measurements of fluid inclusions indicated that the alteration occurred at temperatures similar to the present temperatures. In selected volcaniclastic rocks, excluding andesitic rocks and black shales, clay minerals occurred as glass replacements and pore fillings as seen under SEM and optical microscopy, and exhibited predominantly euhedral hexagonal and elongated forms under TEM, implying that they precipitated *in situ* through hydrolytic reactions of glass and fluid. Based on XRD examination, I-S minerals showed a sigmoidal variation in illite layer percentage (%I) in the range of ~150 to 220ºC and R0 I-S minerals with intermediate %I between 20 and 40% rarely occurred (where R is the Reichweite parameter). The chemical composition also showed a specific variation with depth. Intermediate clays including smectite and I-S minerals are enriched in Al compared to those reported previously from hydrothermal alteration of almost equivalent parent rocks. The oxygen isotope data indicated that the reacting solution was percolating groundwater in the shallow levels and with fossil seawater in the deeper levels. Furthermore, calculating the fluid/rock (W/R) ratio from the isotope variations revealed that the alteration occurred at a nearly constant W/R ratio condition irrespective of %I. Consequently, the observed specific variations in structure and chemical composition of I-S minerals reflect the compositional variations of fluid participating in the crystallization at given temperatures under the conditions of a given original rock and constant W/R ratio. High pH and Na-rich solutions generated by progressive hydrolytic reactions between felsic glass and groundwater favored the precipitation of Al-rich smectite up to ~150ºC and was followed by precipitation of an aluminous R1 I-S mineral with few intermediate R0 I-S minerals at higher temperatures. The crystallization obeys Ostwald's step rule behavior of smectite illitization processes under a high geothermal gradient.

Key Words—Alteration of Felsic Rocks, Fluid-rock Ratio, Illite-smectite Mixed-layer Minerals, Ostwald's Step Rule, Oxygen Isotope, Precipitation.

INTRODUCTION

Dioctahedral clay minerals such as smectite, illite-smectite (I-S) mixed-layer minerals, and illite are widespread as hydrothermal alteration products, so that understanding the crystallization processes of the minerals provides useful information about the thermal and geochemical history during alteration. Sequential distribution from smectite to illite via I-S minerals as a function of temperature, similar to that in burial diagenetic environments, has been documented in many active and extinct hydrothermal systems (Inoue, 1995, and references therein). The formation of I-S minerals is actually affected not only by temperature, but also by other factors such as fluid chemistry, time, fluid/rock (W/R) ratio during the formation of I-S minerals, and chemical composition of the precursor materials (*e.g.* Altaner and Ylagan, 1997). Among the many factors, we tentatively ignore time in the case of the formation of I-S minerals in hydrothermal environments because the formation generally took place over a geologically short period of time, probably during a single event, in contrast to burial diagenesis. Boiling and mixing of fluids in addition to alteration overprint may be more important concerns because they are potentially misleading in terms of the relationship between the observed mineral assemblages and present-day temperature (*e.g.* Patrier *et al.*, 1998).

In the present study, we focus on the formation of dioctahedral minerals during alteration of felsic vitric materials through drill holes near the Kakkonda Geothermal System, Japan. Based on our previous studies (Inoue *et al.*, 2001), the vitric materials in parent volcaniclastic rocks, excluding andesitic rocks and black shales, are assumed to be roughly homogeneous in composition from rhyolitic to dacitic. There was no geological evidence indicating remarkable boiling of fluids and alteration overprint. The aim of this paper is, based on the detailed mineralogical and oxygen isotopic

* E-mail address of corresponding author:
atinoue@earth.s.chiba-u.ac.jp
† Permanent address: Department of Earth Sciences, Chiba University, Chiba 263-8522, Japan
DOI: 10.1346/CCMN.2004.0520108

examinations, to elucidate how glassy materials altered to dioctahedral clay minerals under a given hydrothermal condition and how the structure and chemical and isotopic compositions of product phases were affected by the effects of fluid chemistry and temperature (or thermal gradient) under the conditions of given rock composition and fluid/rock ratio.

GEOLOGICAL BACKGROUNDS OF STUDY HOLES

Kakkonda is an active geothermal system located in the central part of Sengan Basin, Hachimantai, northeast Japan (Figure 1). Here, two power plants have been operated to supply constant electric power of 80 MW since 1978, utilizing relatively shallow (<1500 m) reservoir fluids (Nakamura and Sumi, 1981). By successive drilling exploration, a hidden granitic pluton known as the Kakkonda Granite was recently discovered at >2860 m in Hole WD-1a (Figure 1b). The granite yielded young K-Ar ages of 0.068–0.34 Ma (Kanisawa *et al.*, 1994) and *in situ* temperatures >500ºC inside the body (Muraoka *et al.*, 1998). Thus it is expected to act as a heat source for the deep reservoir system at Kakkonda.

The drill holes studied here are IT-2 and IT-8 drilled at ~5 km east of Kakkonda by NEDO (1993). A schematic geological cross-section along the two drill holes is shown in Figure 2. The pre-Tertiary basement rocks constituting the framework of the Sengan basin structure were encountered by two drill holes adjacent to the study site, WD-1a and AZE-1 (Figure 2). In WD-1a, rocks were contact-metamorphosed by the intrusion of the Kakkonda Granite to form biotite, anthophyllite, andalusite and cordierite (Kato and Sato, 1995). Rocks of AZE-1 consist of chert and slate without the influence of contact metamorphism. The Yamatsuda-Koshidomae and Aniai Formations are marine sediments of Miocene age composed mainly of vitric tuff, tuff breccia, tuffaceous silt to sandstone, and lapilli tuff in the studied holes. The composition of constituent volcanic debris in sediments ranges from rhyolitic to dacitic (Nakamura and Sumi, 1981; NEDO, 1993). The Middle and Lower Aniai Formations contain andesitic tuff breccia and black shale and lignite beds, respectively. The Plio-Pleistocene pyroclastic flow deposits which unconformably overlie the Yamatsuda-Koshidomae Formation consist of rhyolitic to dacitic tuff and tuff breccia with weak welding textures. They are intercalated locally by lacustrine sediments. In addition to thin andesite dikes, a relatively large intrusive body, the Torigoenotaki Dacite, is emplaced between the Kakkonda system and the studied drill holes.

As shown in Figure 3, temperatures measured through IT-2 and IT-8 increase linearly with depth (geothermal gradient $\approx$15–20ºC/100 m) and attain a maximum of 317ºC at the bottom of IT-8 (NEDO, 1993). The linear profile of temperature suggests that there are neither anomalous fluid flows nor boiling of fluids at this location, and the present thermal structure is essentially controlled by conductive heat flow. There was no significant circulation loss during drilling except for a small one at ~920–940 m along the boundary between dike and the surrounding rocks (NEDO, 1993). The two holes studied are insignificant in terms of production of geothermal fluids, although small amounts of hydrothermal fluids were recovered at 1004 m from IT-2.

STUDY SAMPLES AND ANALYTICAL METHODS

Samples

We collected core samples every 5 to 10 m in the ranges of 0–1000 m from IT-2 and 1000 to 1700 m from IT-8, with a total of 268 samples collected. Samples were not collected from levels shallower than 1000 m in IT-8, but as the two drilling sites of IT-2 and IT-8 are very close each other, we regarded them as a continuum of samples from 0 to 1700 m at this location. After routine examination of alteration minerals by thin-section observation and powder XRD analysis, for the present study, samples were selected with particular emphasis on obtaining volcaniclastic rocks with rhyolitic to dacitic vitric materials to minimize the effect of variable chemical compositions in parent rocks. Andesitic rocks, black shales and dike rocks were excluded from the present study of clay minerals. Clay fractions (<2 μm) that were separated from rock samples using ultrasonic vibration and centrifugation were used throughout the present mineralogical and isotopic examinations.

X-ray diffraction and electron microscopic analysis

A step-scanning method at a fixed time of 4 s was used for XRD analysis to examine the nature of interlayering using preferentially oriented samples on glass slides in two air-dried and glycolated states. Samples mounted on Al holders were used to determine the polytypic structure and the d_{060} values. Polytypic structure determination was based on the structure data of muscovite compiled by Bailey (1980). Percentages of illite layers (%I) of I-S clay minerals were determined using convenient techniques developed by Inoue *et al.* (1989) and Watanabe (1981). The results were confirmed by comparing the observed XRD patterns with computer-simulated patterns generated using the NEWMOD program (Reynolds, 1985). The precision of %I determination is usually ±5%, but reduces to ±10% for samples containing more than two types of I-S minerals.

Mineral textures and paragenesis were determined by scanning electron microscopy (SEM), using JEOL JSM-5600LV equipped with an Oxford energy dispersive-type spectrometer (EDS), using freshly broken rock chips sputter-coated with Au. The morphologies of clay

https://doi.org/10.1346/CCMN.2004.0520108 Published online by Cambridge University Press

minerals also were observed under a Hitachi H-7100FA transmission electron microscope (TEM).

Chemical analysis

Electron microprobe analysis was carried out on the flat surfaces of clay pellets, prepared by pressing the separated powder, using a JEOL JSM-5600 equipped with an Oxford Link EDS detector operating with an accelerating voltage of 15 kV, a beam current of 0.8 nA, an analytical area of 5×5 μm, and a counting time of 100 s. The ZAF correction of the EDS data obtained was made by a Link ISIS system calibrated with synthesized oxides and natural minerals as standards. Chemical analyses were performed on more than 10 points on the clay pellet and, using the averaged values, were cast into the structure formula on the basis of $O_{10}(OH)_2$. Although XRD examination showed that some of the samples used were inevitably contaminated by trace amounts of impurities, the effect of contamination was ignored in the calculations of structure formulae. All the Fe determined was calculated as ferric iron. The exchangeable and non-exchangeable interlayer cations were distinguished in the calculations of the structure formulae using the independent exchangeable cation measurements described below. The precision of microprobe analysis is better than ±2% for all the elements measured. However, some of the analyzed samples contained trace amounts of impurities and/or were a mixture of I-S minerals with different %I. Note that the data represent the bulk composition of separated clay fractions.

The exchangeable interlayer cation composition of clays was determined following Inoue (2000). About 0.1 g of clay sample were placed in a polyethylene bottle with 50 mL of 0.1 N strontium chloride to extract exchangeable cations from the interlayer positions of clay minerals. After keeping the bottles at room temperature for one day, the suspension was separated into solid and solution phases by centrifugation. Then Na, K, Mg and Ca in the supernatant liquid were analyzed as exchangeable cations of the clay by atomic absorption spectroscopy. The precision of exchangeable cation measurements is better than 0.5 meq/100 g clay for all the elements.

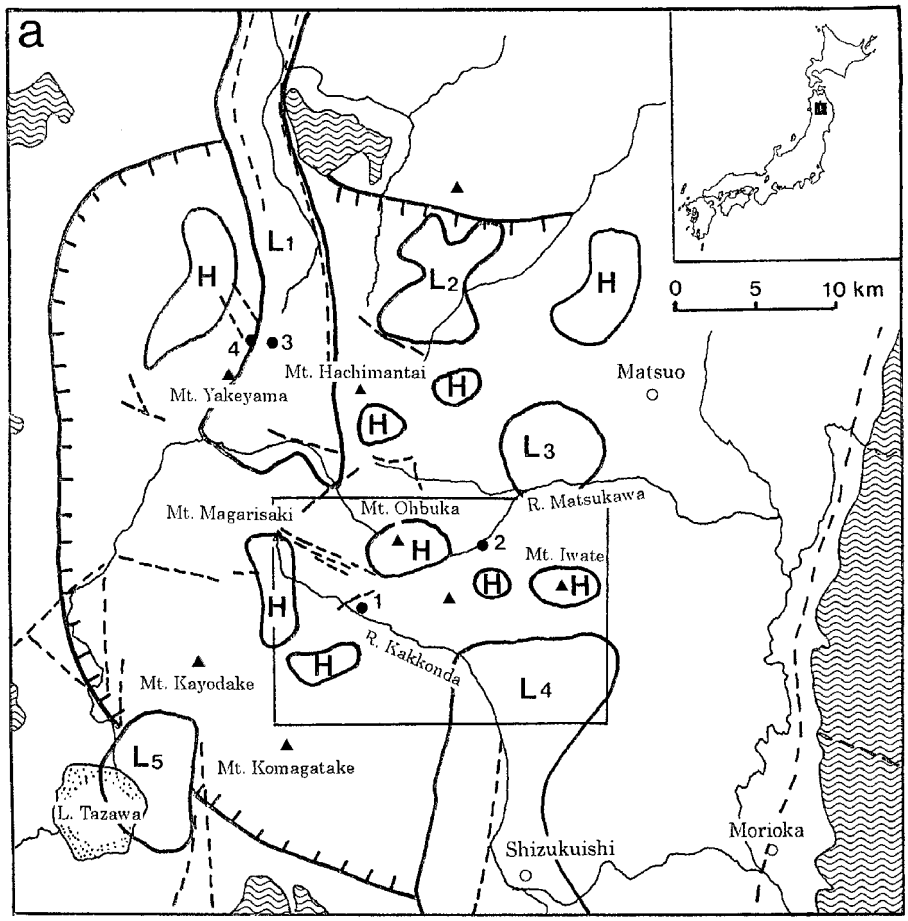

Figure 1. (*This and opposite page*) Structure map of the Hachimantai volcanic area, together with Bouguer anomaly area (a) and geologic map of the Kakkonda area and locations of drill holes studied (b), which was simplified from NEDO (1993).

https://doi.org/10.1346/CCMN.2004.0520108 Published online by Cambridge University Press

Oxygen isotope analysis

The clay samples prepared for oxygen isotope analysis were the same as those for XRD and chemical analyses. Oxygen isotope analyses were obtained by the BrF_5 method (Clayton and Mayeda, 1963); the analyses were performed at CRPG-CNRS (Nancy, France). Isotopic data are reported in the $\delta^{18}O$ notation, $\delta^{18}O = [(R_{sample}/R_{standard}) - 1] \times 1000$, where $R = {}^{18}O/{}^{16}O$; they are reported relative to SMOW (Standard Mean Ocean Water). The precision of $\delta^{18}O$ measurements is better than ±0.2‰. The presence of impurities in the samples used for the $\delta^{18}O$ measurements was ignored because of their small amounts.

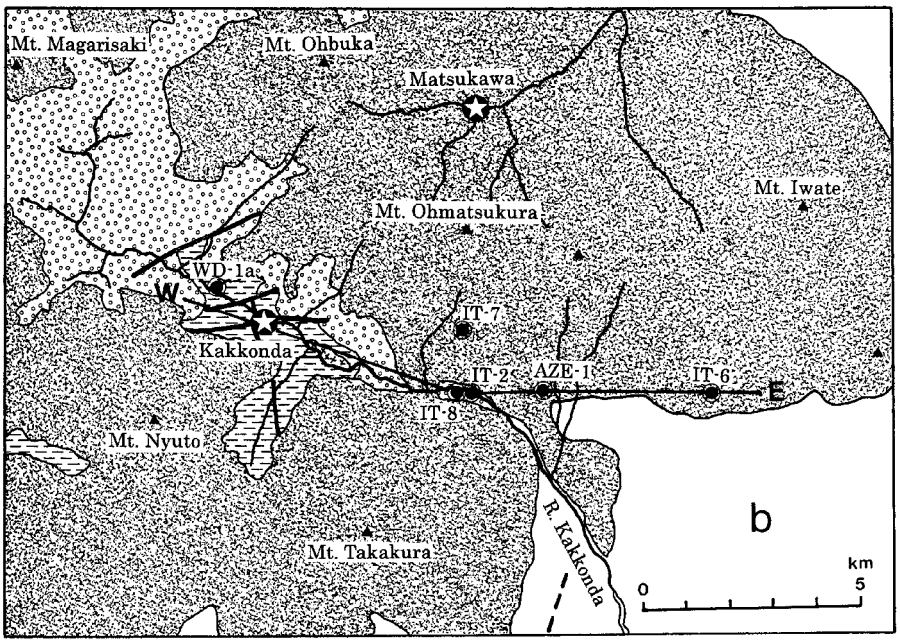

Legend of (a) and (b)

- Alluvial deposits
- Quaternary volcanic rocks
- Plio-Pleistocene pyroclastic sediments
- Yamatsuda and Koshidomae Formations
- Upper Aniai Formation
- Middle Aniai Formation
- Lower Aniai Formation
- Pre-Tertiary rocks
- Kakkonda Granite (hidden)
- Dike/Intrusive rocks
- Sengan Basin
- H: High Bouguer anomaly area
- L: Low Bouguer anomaly area
- L_1: Hanawa area
- L_2: Appi-Kusanoyu area
- L_3: Matsuo area
- L_4: Shizukuishi area
- L_5: Tazawako area
- Geothermal power plant
  - 1: Kakkonda
  - 2: Matsukawa
  - 3: Ohnuma
  - 4: Sumikawa
- Faults
- Drillholes

https://doi.org/10.1346/CCMN.2004.0520108 Published online by Cambridge University Press

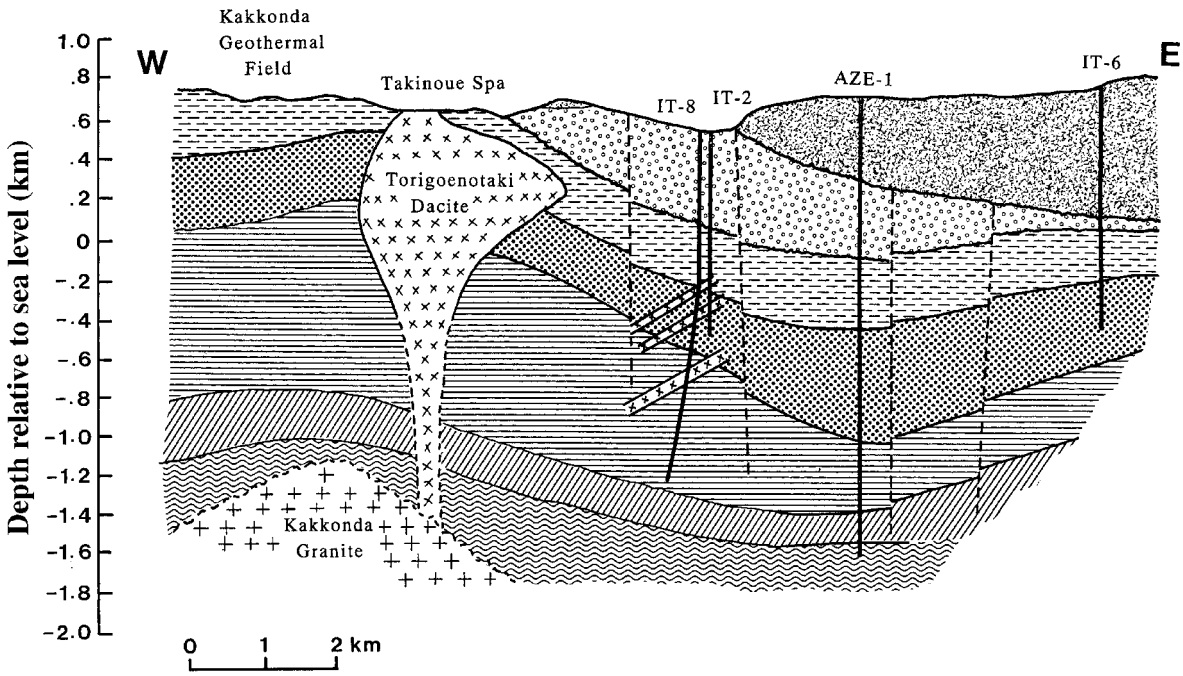

Figure 2. Schematic geologic cross-section along the E–W line of Figure 1. See the legend of Figure 1 for symbols of stratigraphic units.

Estimation of fluid/rock ratios

It is possible to estimate fluid/rock (W/R) ratio during alteration from oxygen isotope variations (Taylor, 1974). However, the ratios obtained depend strongly on the alteration model adopted in the calculations. According to the mode of occurrence of the clay minerals, as will be described below, we assumed here a simple model for the formation of clay minerals based on dissolution of glass and subsequent precipitation of clays in a closed system (see Appendix). In this model, it is an important assumption that the dissolving reactant is in disequilibrium, while the precipitating products are in equilibrium with the system. Moreover, it was assumed that the initial values of $\delta^{18}O$ of rock and fluid prior to alteration are 7‰ and −11‰, respectively. The former value (7‰) was cited from the compilation of Matsuhisa (1979) for Cenozoic igneous rocks in this area. The $\delta^{18}O_{fluid}$ of −11‰ is a mean value of meteoric waters in this area (Inoue *et al.*, 2001).

GENERAL DESCRIPTIONS OF ALTERATION AND FLUID GEOCHEMISTRY

Based on bulk rock mineralogy of IT-2 and IT-8 (Figure 3), the alteration is characterized by the following zoning of Na-rich silicate minerals from the surface to the bottom: smectite + unaltered glass (<260 m, <78ºC) → clinoptilolite + smectite (~260–560 m, ~78–140ºC) → mordenite + smectite (~390–580 m, ~101–143°C) → analcime + smectite or I-S (~532–664 m, ~133–160ºC) → albite + I-S or illite (>750 m, >174ºC), where the temperatures in parentheses are cited from the present-day measurements. The boundary temperatures of zeolite zones are in agreement with those estimated from alteration of silicic tuff in Yucca Mountain reported by Bish and Aronson (1993). It is also noted that the boundary temperature (~170ºC) of analcime (+ quartz) and albite is close to that determined experimentally by Thompson (1971).

The zoning is subparallel to the formation boundaries and is developed continuously from the upper non-marine formation to the lower marine formations without interruption by the unconformity. The alteration minerals generally occurred as glass replacements and pore fillings, but not as veins (Figure 4). Primary plagioclase (oligoclase to andesine) was rarely replaced by clay minerals and zeolites through IT-2. They remained unaltered above a depth of 750 m, although the phenocrysts contained intensive dissolution pores from ~600–750 m. Below 750 m, pure albite overgrew along the fringes of dissolution pores together with the precipitation of euhedral albite crystals in the interstitial pore spaces of matrix (Figure 4d). Secondary K-feldspar was detected only locally in the deeper levels. K-feldspar in Plio-Pleistocene pyroclastic rocks is possibly one of the recrystallization products due to intensive welding. Corrensite (Figure 4e) filled pore spaces intimately with I-S or illitic minerals in the limited range ~740–1060 m (~172–229ºC). Kaolinite was identified at local horizons such as lacustrine deposits and the unconformity. Small amounts of kaolinite also occurred around 700 m; it exhibited

https://doi.org/10.1346/CCMN.2004.0520108 Published online by Cambridge University Press

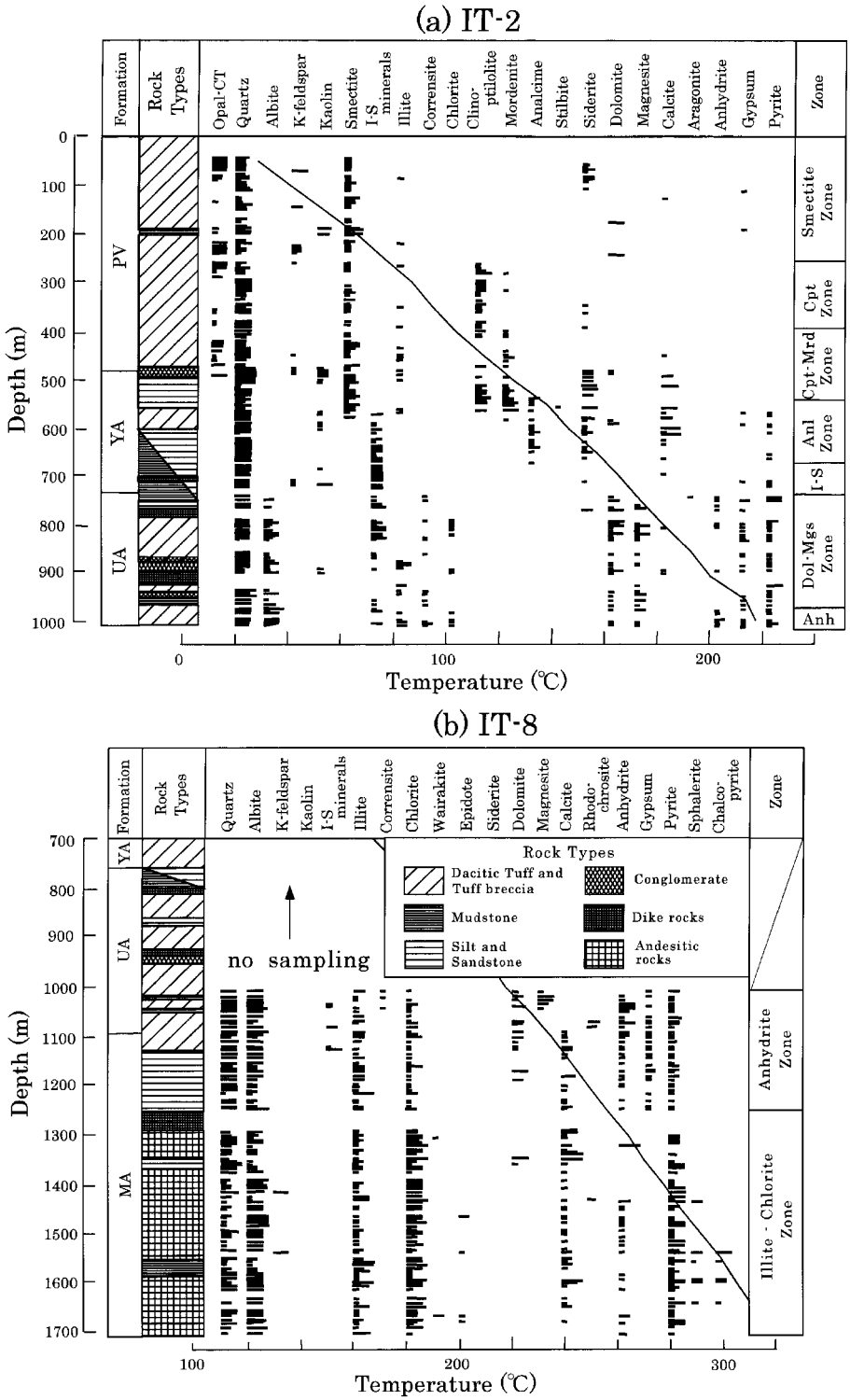

Figure 3. Distribution of secondary minerals in IT-2 (a) and IT-8 (b). The lengths of the bars represent the qualitative abundance of the minerals. The curves in the figures are the present-day temperatures. Cpt: clinoptilolite, Mrd: mordenite, Anl: analcime, Dol: dolomite, Mgs: magnesite, Anh: anhydrite, I-S: illite-smectite minerals.

euhedral shapes and was grown on the flakes of I-S minerals (Figure 4f), suggesting a later product after the crystallization of I-S minerals.

The above zoning also is overlapped by the zonal distribution of carbonate, sulfate and sulfide (Figure 3). In reference to the present study, it is noted that dolomite

https://doi.org/10.1346/CCMN.2004.0520108 Published online by Cambridge University Press

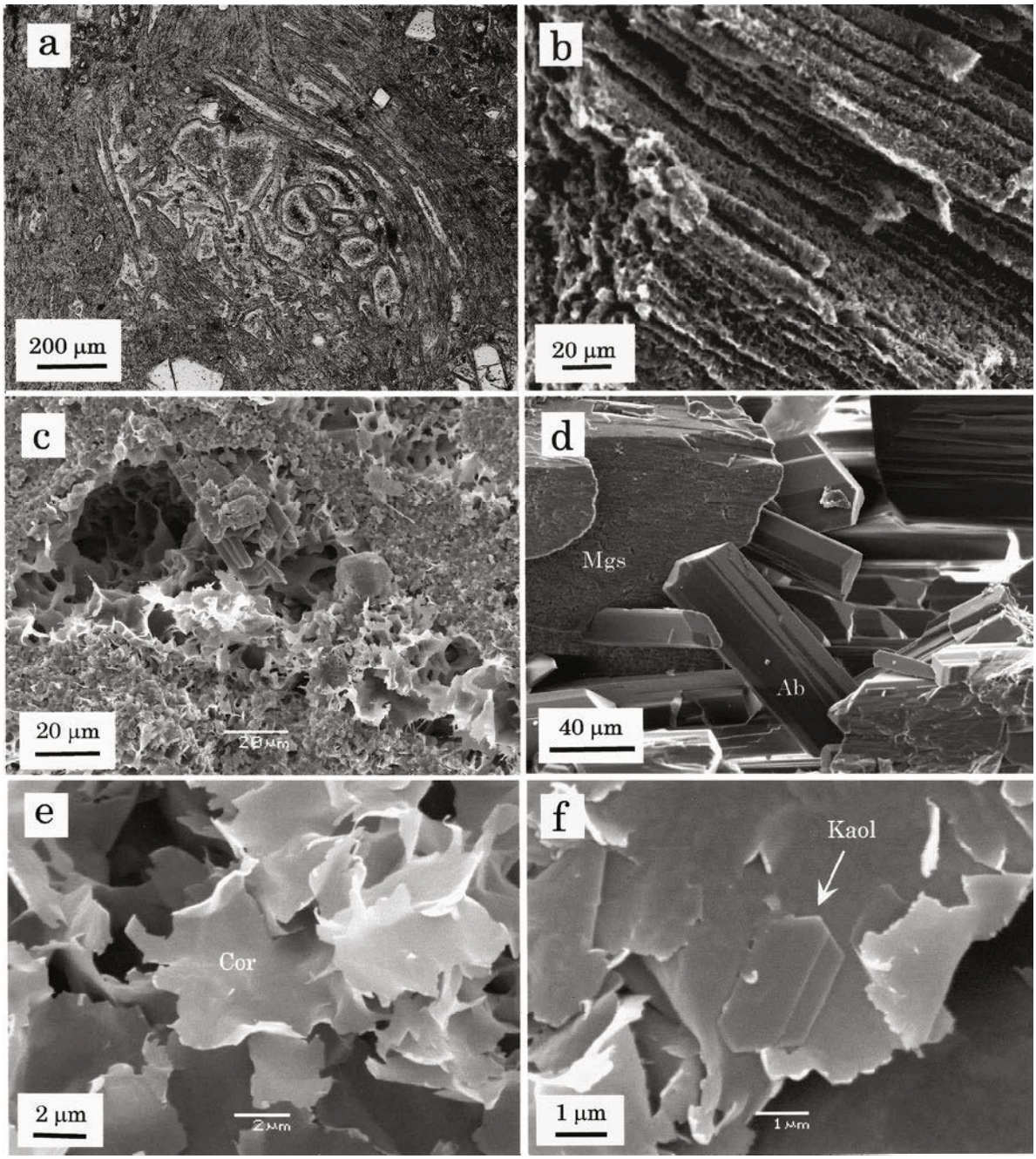

Figure 4. Optical and SEM photomicrographs showing the occurrence of altered minerals: (a) smectite and clinoptilolite occupying vesicles of pumice, (b) smectite pseudomorphically replacing pumice wall, (c) I-S minerals precipitated in pore spaces in volcanics, (d) euhedral albite (Ab) and magnesite (Mgs) occupying pore spaces, (e) corrensite (Cor) precipitated in pore spaces in volcanics, (f) kaolinite crystals (Kaol) grown on I-S flakes.

and magnesite predominated from ~740–1190 m associated with euhedral crystals of albite (Figure 4d), corrensite, and/or chlorite. Anhydrite was widespread from 973 m to the bottom of IT-8. The compositional variations of carbonate minerals were described by Inoue *et al.* (2001).

The homogenization temperatures of fluid inclusions in secondary quartz, calcite and anhydrite were plotted along the depth profiles of present-day temperature (NEDO, 1993; Inoue *et al.*, 2001), implying that the alteration minerals probably formed at temperatures similar to the present temperatures. The measured homogenization temperatures were always lower than those of the boiling point of pure water at respective depth, assuming hydrostatic pressure (Inoue *et al.*, 2001).

https://doi.org/10.1346/CCMN.2004.0520108 Published online by Cambridge University Press

Table 1. Chemical and isotope compositions of hydrothermal solution recovered from 1004 m from IT-2 and the calculated logarithmic activities at *in situ* temperature.

	Observed (NEDO, 1993)	Calculated (Inoue *et al.*, 2001)
Temperature (ºC)	218	
pH (room temp.)	7.3	$\log a_H = -6.3$
Na (mg/L)	2820	$\log a_{Na} = -1.2$
Ca (mg/L)	9.5	$\log a_{Ca} = -4.8$
K (mg/L)	51.0	$\log a_K = -3.2$
Mg (mg/L)	1.1	$\log a_{Mg} = -5.4$
SiO_2 (mg/L)	397	$\log a_{SiO_2} = -2.3$
Al (mg/L)	9.7	
B (mg/L)	48.7	
HCO_3 (mg/L)	1340	$\log a_{CO_2(total)} = -1.6$
Cl (mg/L)	3420	
SO_4 (mg/L)	286	$\log a_{SO_4} = -3.6$
δD (‰)	−48.9	−55.3
$\delta^{18}O$ (‰)	−4.0	−5.2
$\delta^{13}C$ (‰)	−2.3	
$\delta^{34}S$ (‰)	19.6	
Tritium (TR units)	<0.9	

Hydrothermal fluid, NaCl-rich saline type (Table 1), was recovered at 1004 m from IT-2. Based on the cation activity ratios, Inoue *et al.* (2001) demonstrated that the fluid was in chemical equilibrium with respect to muscovite, albite, chlorite, dolomite and quartz, but slightly undersaturated with magnesite, calcite and anhydrite at *in situ* temperature (218ºC). From comparison of the solute and isotope composition with those of related waters around the Kakkonda area, the recovered fluid differs in origin from hydrothermal fluids circulating in the Kakkonda system and is probably a stagnant, mixed solution of meteoric water and fossil seawater trapped in the Miocene Aniai formations (Inoue *et al.*, 2001).

RESULTS

X-ray diffraction

Representative XRD patterns of the clay samples examined are illustrated in Figure 5. Samples from near-surface to ~635 m are smectite and R0-type I-S. Smectite from ~125–320 m showed a decrease in expandability to some extent based on the saddle/001 peak intensity method (Inoue *et al.*, 1989). The samples showed a relatively larger full width at half maximum of the 001 reflection and the higher-order reflections were hardly observed compared to samples from deeper levels. This suggests that smectite samples from the near-surface have a smaller coherent domain size (or number of layers) than that in smectite from deeper levels. Some samples (*e.g.* from 645 m) are a mixture of

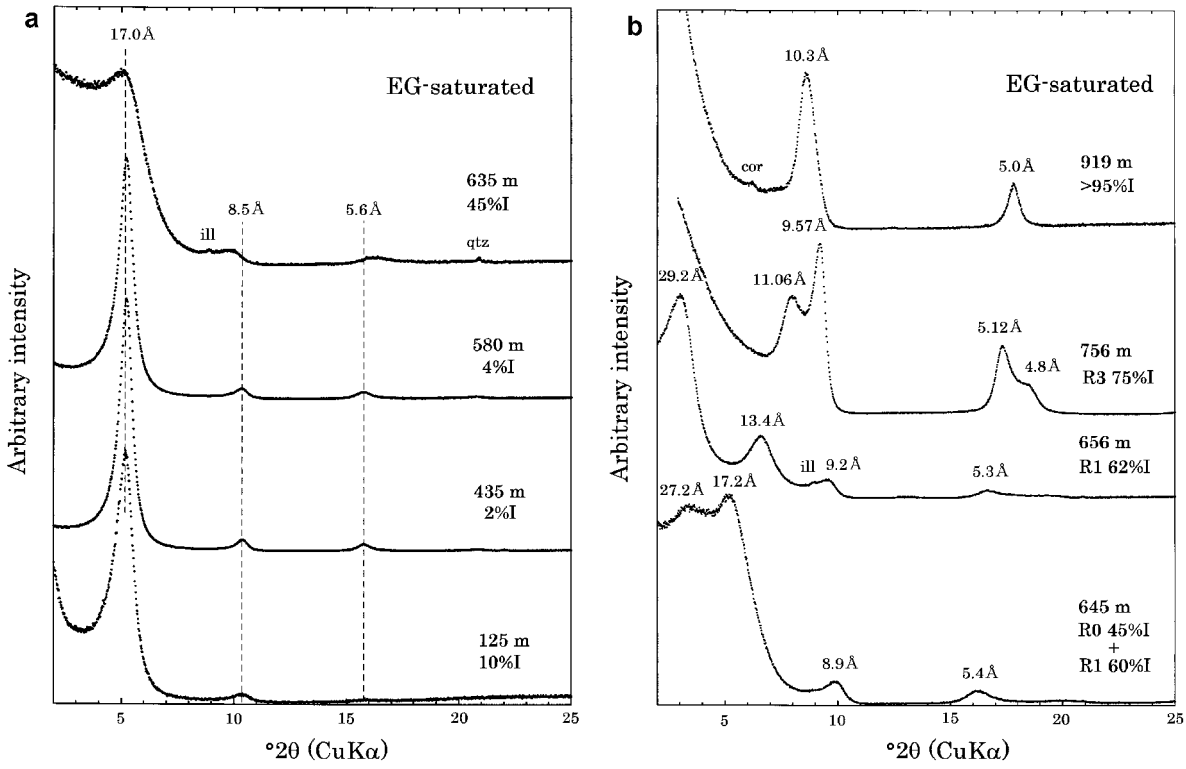

Figure 5. Representative XRD patterns of the studied samples after ethylene glycol (EG)-saturation: (a) smectite and R0 type of I-S, (b) R1, R0 + R1 types of I-S, R3 type of I-S, and illite from various depths of drill hole IT-2. The illite layer percentages were determined using the techniques of Inoue *et al.* (1989) and Watanabe (1981). ill: illite, qtz: quartz, cor: corrensite.

https://doi.org/10.1346/CCMN.2004.0520108 Published online by Cambridge University Press

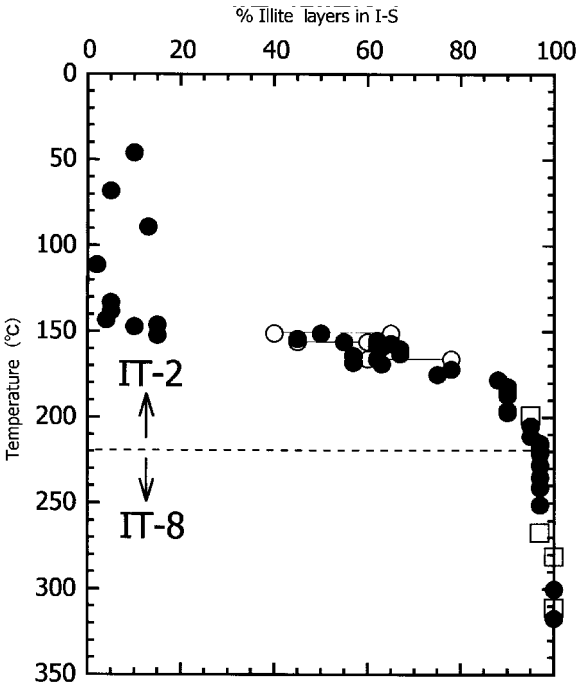

Figure 6. Variation of %I in I-S minerals as a function of the present-day temperature in IT-2 and IT-8. The tie lines between open circles indicate the presence of more than two I-S samples with different %I in a rock specimen. Squares indicate the %I data of I-S minerals obtained from andesitic rocks in the Aniai Formation.

R0 and R1. Illite-smectite minerals from ~640–740 m and from ~740–900 m were identified as R1 and R3 ordered structures, respectively. The variation of %I determined is plotted as a function of the present-day temperature in Figure 6. The %I values increase with temperature from about 150ºC to ~220ºC, but the increase seems to be discontinuous so as to display a gap between ~20 and 40%I. More than two types of I-S minerals coexist at intermediate stages. True illite without any expandability appears at ~250ºC. As the %I data of I-S minerals obtained from thin felsic sediments and andesitic rocks in the Middle Aniai Formation were plotted in Figure 6 for comparison, they showed a smooth variation following the previous trend of I-S minerals.

X-ray diffraction patterns of the randomly oriented samples (not presented here) showed that I-S minerals with <50%I were characterized by a turbostratic structure caused by random rotation of layers and those with >50%I basically had a 1*M* polytype structure. The *hkl* reflections corresponding to 1*M* polytype structure became sharp in I-S minerals with >75%I (*e.g.* 756 m sample), but broadened in those with ~50–75%I. Thus the latter may be classified as $1M_d$. The 1559 m sample, which is pure illite, was a mixture of 1*M* and $2M_1$ based on the indexing of *hkl* reflections. The d_{060} values were almost constant at ~1.497–1.500 Å throughout the entire I-S series.

Chemical composition

Chemical composition, determined by electron microprobe analysis, is given in Table 2. Some unrealistic values in the calculated structure formulae for some samples were due to the presence of impurities. The low total weight percent values were attributed mainly to the surface roughness of prepared clay pellets. Despite the imprecision, the chemical variation in the 2:1 silicate layer can be qualitatively represented in the triangle diagram of pyrophyllite, muscovite and celadonite as shown in Figure 7. Ferric iron was regarded as substituting for Al in the figure. Smectite from the near-surface (*e.g.* 125 m sample) is classified as an Fe-rich beidellite-montmorillonite solid-solution. The smectite composition becomes montmorillonitic at ~320–435 m and then beidellitic at 580 m, accompanying a small increase in total layer charge. The compositions of I-S minerals are much more aluminous between 600 m and 700 m and then become enriched in Mg below 740 m (*e.g.* 756 m sample), the depth which corresponds to the first appearance of dolomite and magnesite (Figure 3). The almost pure illites at 919 m and 1559 m have a phengitic composition with more than $-0.75/O_{10}(OH)_2$ of total layer charge. Illite and the illite component of I-S minerals show some solid-solution with paragonite, taking account of the non-exchangeable Na content (Table 2).

Figure 8 shows the variations of exchangeable cation composition of clay samples as a function of depth. The clays from near-surface are enriched in Ca and Mg and depleted in Na and K as the exchangeable interlayer cation. The Ca and Mg contents decrease and the Na content increases concomitantly with depth down to ~300 m at which level clays coexist with clinoptilolite. The Na content in clay samples stays constant at a high level (>0.7 in equivalent fraction) between ~300 and 750 m, higher still in the analcime zone. Below ~750 m, however, the Na content decreases again with depth, concomitant with increasing Mg. The exchangeable K content is always low throughout the rock column of IT-2.

SEM and TEM observations

Scanning electron microscopy observations showed that in near-surface rocks, smectite occurred as partial replacements of glass shards and pumice wall (Figure 9a) and pore-fillings often associated with goethite and opal. In deeper rocks, glassy materials are totally replaced by smectite (Figures 4b and 9b). The occurrence of I-S and illite was almost the same as those of smectite, *i.e.* pore fillings and glass replacements. They show a hair or filament texture and stiffer, thicker filaments or laths aggregate textures under SEM, depending on %I (Figure 9c and d).

Figure 10 shows TEM images of I-S minerals. They display a morphological change from flaky to lath-shaped with increasing %I, while they tended to increase

https://doi.org/10.1346/CCMN.2004.0520108 Published online by Cambridge University Press

Table 2. Chemical compositions of smectite, I-S minerals, and illite in drill holes IT-2 and IT-8 of the Kakkonda geothermal field.

Samples	2-125	2-214	2-320	2-435	2-580	2-635	2-645	2-656	2-664	2-680	2-690	2-700	2-756	2-873	2-879	2-919	8-1559
Analyzed points	11	10	10	10	10	10	10	11	12	10	15	12	10	14	10	13	13
SiO_2	58.42	60.30	63.43	58.50	57.47	59.37	52.41	51.39	50.09	51.67	46.66	51.14	49.64	46.61	49.16	46.53	48.03
Al_2O_3	12.54	18.72	19.97	18.12	24.29	26.43	30.07	28.95	29.64	27.45	29.07	30.29	28.92	24.37	26.43	27.48	28.37
TiO_2	0.88	0.40	0.40	0.44	0.12	0.54	0.10	0.27	0.27	0.42	0.05	0.09	0.02	0.12	0.09	0.00	0.07
Fe_2O_3	15.66	6.56	5.41	6.87	3.77	2.61	1.61	1.97	1.76	1.86	1.35	1.05	0.18	1.35	1.79	1.71	1.75
MgO	2.39	2.50	3.57	2.93	1.95	1.01	0.91	0.96	0.88	0.92	0.80	0.90	2.15	2.29	2.02	2.34	2.40
CaO	1.50	0.70	0.31	0.56	0.09	0.92	0.30	0.05	0.01	0.05	0.12	0.11	0.03	0.73	0.26	0.02	0.01
Na_2O	0.88	2.27	2.78	2.62	3.33	3.08	2.39	1.80	1.83	1.41	1.62	1.72	1.05	0.76	0.67	0.56	0.60
K_2O	0.38	0.47	1.06	0.51	0.28	2.04	3.06	5.05	5.35	5.84	4.80	5.38	6.68	6.25	6.63	7.32	7.43
Total	92.66	91.91	94.93	90.55	91.29	95.99	90.84	90.45	89.84	89.60	84.47	90.68	88.67	82.49	87.04	85.97	88.66
On the basis of $O_{10}(OH)_2$																	
Tetrahedral																	
Si	3.91	3.93	4.00	3.90	3.75	3.71	3.48	3.47	3.41	3.53	3.37	3.44	3.43	3.49	3.48	3.36	3.36
Al	0.09	0.07	0.00	0.10	0.25	0.29	0.52	0.53	0.59	0.47	0.63	0.56	0.57	0.51	0.52	0.64	0.64
Layer charge	−0.09	−0.07	0.00	−0.10	−0.25	−0.29	−0.52	−0.53	−0.59	−0.47	−0.63	−0.56	−0.57	−0.51	−0.52	−0.64	−0.64
Octahedral																	
Al	0.90	1.37	1.33	1.32	1.62	1.66	1.83	1.77	1.79	1.74	1.84	1.84	1.79	1.64	1.69	1.70	1.70
Fe^{3+}	0.79	0.32	0.26	0.35	0.19	0.13	0.08	0.10	0.09	0.10	0.08	0.06	0.01	0.08	0.10	0.10	0.09
Mg	0.19	0.23	0.32	0.28	0.19	0.19	0.09	0.10	0.09	0.09	0.07	0.09	0.22	0.20	0.19	0.25	0.25
Ti	0.04	0.02	0.02	0.02	0.01	0.03	0.01	0.02	0.02	0.02	0.01	0.01	0.00	0.01	0.01	0.00	0.01
Sum	1.92	1.94	1.93	1.97	2.01	2.01	2.01	1.99	1.99	1.95	2.00	2.00	2.02	1.93	1.99	2.05	2.05
Layer charge	−0.39	−0.39	−0.51	−0.35	−0.15	−0.13	−0.05	−0.11	−0.10	−0.22	−0.06	−0.08	−0.16	−0.40	−0.21	−0.10	−0.09
Total layer charge	−0.48	−0.46	−0.51	−0.45	−0.40	−0.42	−0.57	−0.64	−0.69	−0.69	−0.69	−0.64	−0.73	−0.91	−0.73	−0.74	−0.73
Non-exchangeable Interlayer																	
K	0.02	0.03	0.06	0.03	0.02	0.15	0.24	0.42	0.45	0.49	0.42	0.44	0.58	0.58	0.58	0.67	0.67
Na	0.10	0.08	0.08	0.09	0.04	0.19	0.06	0.06	0.09	0.08	0.05	0.08	0.08	0.10	0.08	0.06	0.08
Ca	0.03	0.02	0.00	0.02	0.00	0.02	0.00	0.00	0.00	0.00	0.00	0.00	0.00	0.00	0.00	0.00	0.00
Mg	0.00	0.00	0.00	0.00	0.00	0.00	0.00	0.00	0.00	0.00	0.00	0.00	0.00	0.00	0.00	0.00	0.00
Layer charge	0.18	0.15	0.14	0.16	0.06	0.38	0.30	0.48	0.54	0.57	0.47	0.52	0.66	0.68	0.66	0.73	0.75
Exchangeable Interlayer																	
K	0.01	0.01	0.02	0.02	0.01	0.02	0.02	0.02	0.02	0.02	0.02	0.02	0.01	0.02	0.02	0.01	–
Na	0.01	0.18	0.26	0.25	0.38	0.18	0.24	0.17	0.15	0.10	0.17	0.14	0.06	0.01	0.01	0.02	–
Ca	0.08	0.03	0.02	0.02	0.01	0.04	0.02	0.01	0.01	0.01	0.01	0.01	0.01	0.04	0.02	0.00	–
Mg	0.05	0.02	0.01	0.01	0.00	0.01	0.00	0.00	0.00	0.01	0.01	0.00	0.00	0.06	0.02	0.00	–
Layer charge	0.28	0.29	0.34	0.33	0.41	0.30	0.30	0.21	0.19	0.16	0.23	0.18	0.09	0.23	0.11	0.03	–
Total layer charge	0.46	0.44	0.48	0.49	0.47	0.68	0.60	0.69	0.73	0.73	0.70	0.70	0.75	0.91	0.77	0.76	0.75
%I	10	5	13	2	4	45	45+60	62	67	67	57	60+78	75	90	90	>95	100
CEC (meq/100 g)	71.4	77.6	88.3	86.1	108.4	78.6	81.6	50.8	49.3	40.2	56.5	48.3	25.6	54.7	30.0	25.2	–
Impurities		pl	opal-CT cpt	qz	qz	qz ill		qz ill	qz	qz				qz, ab dol, mgs	qz, ab, cor	qz, cor, ab	chl

pl: plagioclase, cpt: clinoptilolite, qz: quartz, ill: illite, ab: albite, dol: dolomite, mgs: magnesite, cor: corrensite, chl: chlorite

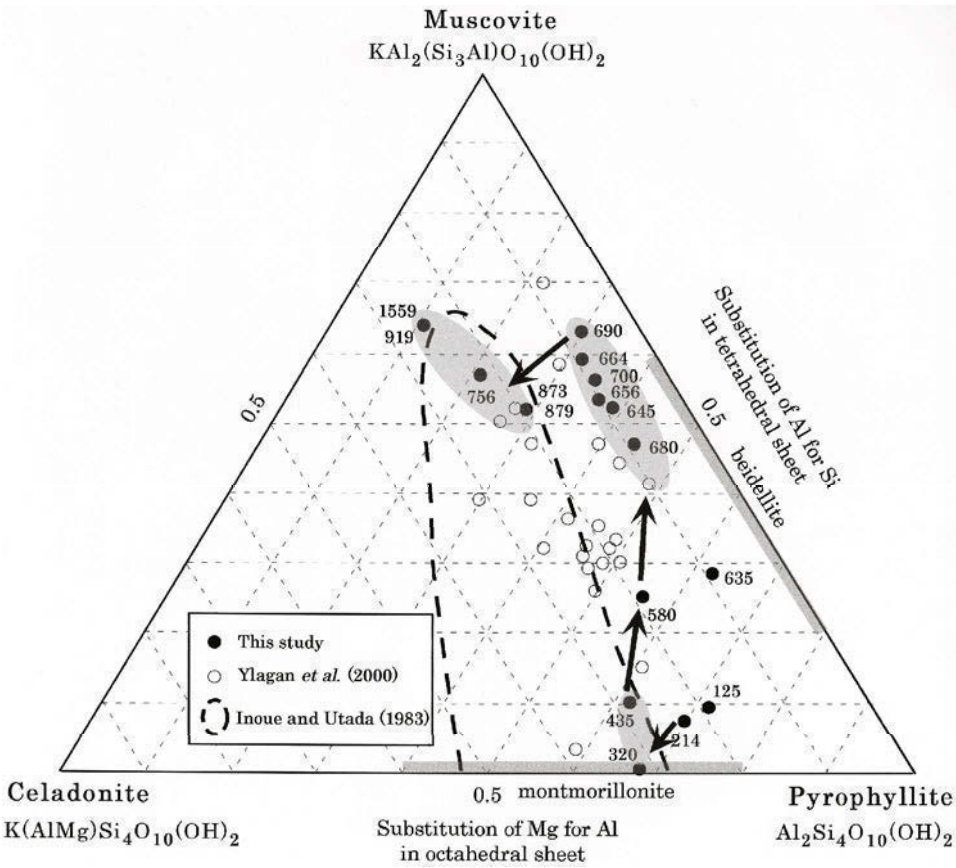

Figure 7. Triangular plots of chemical compositions of I-S minerals. The appended numbers correspond to the depths of samples. Arrows indicate the chemical variations as a function of depth. Samples 645 m and 700 m are a mixture of R0 and R1 structures. Sample 635 m is contaminated by quartz as seen in Figure 5.

slightly in crystal size based on the preliminary measurements on TEM images. It is noteworthy that I-S minerals from 635 m (R0 45%I) and 664 m (R1 67%I) samples contain significant amounts of euhedral crystals with distinct forms of hexagonal flake and elongated lath. Both euhedral crystals are thought to be neoformed *in situ* by direct precipitation from solution, but not to replace precursor smectite.

Oxygen isotope variation

The $\delta^{18}O$ values of clay samples determined, together with the $\delta^{18}O$ values of coexisting carbonates determined previously (Inoue *et al.*, 2001), are given in Table 3. The $\delta^{18}O$ values of clays decrease with increasing depth (or temperature) from 12.6‰ at 214 m (68ºC) to 6.2‰ at 873 m (196ºC), as illustrated in Figure 11. The %I of the samples ranges from 2 to ~90%.

If it is assumed that I-S minerals were isotopically equilibrated with fluids at given temperatures, the $\delta^{18}O$ values of equilibrated fluids can be evaluated using an oxygen isotope fractionation equation between I-S and water proposed by Savin and Lee (1988) as a function of temperature and %I:

$$\Delta_{I/S\text{-}w} = \delta^{18}O_{I/S} - \delta^{18}O_{fluid} = 10^3 \ln\alpha = (2.58 - 0.19I)(10^6 T^{-2}) - 4.19 \quad (1)$$

where I is the fractional content of illite layers in I-S minerals and T is the temperature in Kelvin. Using the present-day temperatures and %I values determined, the $\delta^{18}O$ values of fluids were calculated from equation 1 as given in Table 3 and Figure 11. The calculated $\delta^{18}O$ values of fluids equilibrated with coexisting carbonate minerals (Inoue *et al.*, 2001) are also appended in the figure. It is obvious that the calculated $\delta^{18}O_{fluid}$ values follow a smooth curve, irrespective of minerals, implying that the secondary minerals precipitated simultaneously from a common fluid and were probably in isotopic equilibrium with the fluid.

The upward extrapolation of the $\delta^{18}O_{fluid}$ plots extends around −11‰ at the surface. The value coincides with the $\delta^{18}O$ of meteoric water (−10 to −12‰) in this area (Inoue *et al.*, 2001). Thus, the reacting solution is basically of meteoric origin, supporting our previous conclusion; the observed isotopic variations were caused by the degree of fluid-rock interaction at different temperatures. On the other hand (>873 m), though few in number, the $\delta^{18}O$ values

https://doi.org/10.1346/CCMN.2004.0520108 Published online by Cambridge University Press

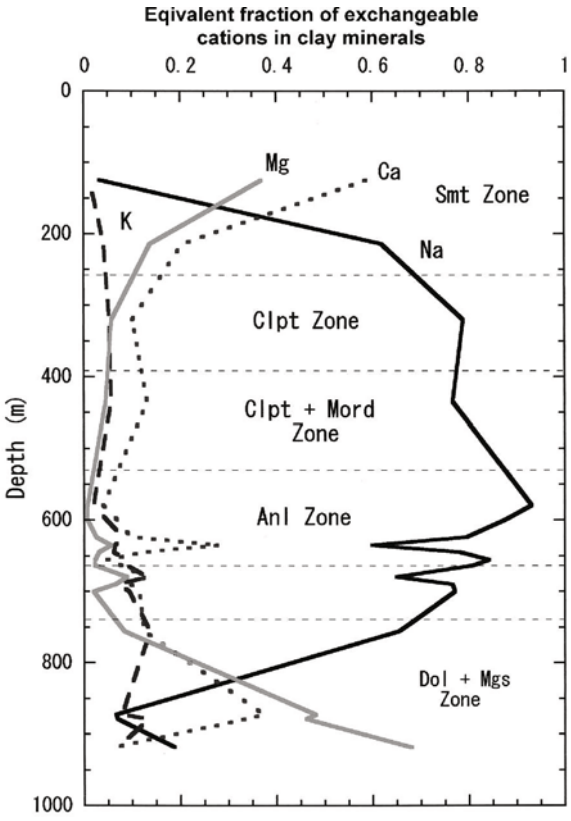

Figure 8. Variation of exchangeable interlayer cations in clay samples as a function of depth, expressed as an equivalent fraction of the total exchangeable cation. Thin dashed lines delineate each mineral zone. Smt: smectite, Clpt: clinoptilolite, Mord: mordenite, Anl: analcime, Dol: dolomite, Mgs: magnesite.

of fluids equilibrated with less expandable I-S, illite, and calcite seem to be constant at −0.6‰. This value is close to the seawater values (~0‰) rather than the $\delta^{18}O$ value (−5.2‰) of hydrothermal fluid recovered at 1004 m of IT-2 (Table 1).

Fluid/rock (W/R) ratios

Assuming an alteration model (Appendix), the evaluated W/R mass ratios are constant at ~0.3 on average, irrespective of %I (Table 3). This value is smaller than those (0.5–2.0) given previously for active and extinct hydrothermal systems (Larson and Taylor, 1986; White *et al*., 1992). Christidis (1998) reported still greater W/R ratios (0.9–13.3) for the smectitization of volcanic glass in Milos Island based on mass-balance calculations. The value should be regarded as tentative, based on many assumptions, but we can say in the present study that the alteration took place at nearly constant W/R ratio.

DISCUSSION

Crystallization of clay minerals

The textural evidence of clay minerals under SEM and TEM, in addition to the thin-section observations, indicates that glass was dissolved by hydrolytic reaction and the clay minerals precipitated *in situ*. The $\delta^{18}O_{fluid}$ evaluated from the alteration minerals supports the meteoric origin of fluids participating in the alteration at least at shallower levels (<740 m).

Under oxidative conditions at the near-surface, the reaction of glass with percolating groundwater favored the formation of Fe-beidellitic smectite together with goethite or with siderite under increased f_{CO_2} conditions.

Table 3. Oxygen isotope data of clays and carbonates in IT-2 and IT-8 and evaluated fluid/rock (W/R) mass ratios.

Samples	Minerals	%I (Reichweite)	Temp. (ºC)	$\delta^{18}O_{mineral}$ (‰)	$\delta^{18}O_{fluid}$* (‰)	W/R** (mass unit)
IT-2-214	smectite	5 (R0)	68	12.6	−5.3	0.09
IT-2-320	smectite	13 (R0)	89	8.4	−6.9	0.59
IT-2-435	smectite	2 (R0)	111	9.2	−4.1	0.21
IT-2-510	siderite	–	128	13.3	−2.6	–
IT-2-580	smectite	4 (R0)	143	7.1	−3.6	0.28
IT-2-635	I-S	45 (R0)	154	6.8	−2.7	0.28
IT-2-645	I-S	45+60 (R0+R1)	156	6.2	−3.1	0.33
IT-2-656	I-S	62 (R1)	158	6.1	−3.0	0.33
IT-2-664	I-S	67 (R1)	160	5.6	−3.2	0.38
IT-2-690	I-S	57 (R1)	164	5.9	−2.9	0.33
IT-2-700	I-S	62 (R1)	166	6.7	−1.9	0.25
IT-2-756	I-S	75 (R3)	175	5.6	−2.4	0.32
IT-2-815	dolomite, magnesite	–	186	10.6	−1.9	–
IT-2-873	I-S	90 (>R3)	196	6.2	−0.6	0.21
IT-8-1591	calcite	–	304	4.7	−0.6	–

* The $\delta^{18}O_{SMOW}$ values of fluids equilibrated with clays were calculated using the fractionation equation of Savin and Lee (1988) and those for carbonates were cited from Inoue *et al*. (2001).
** The W/R values correspond to the fluid:rock mass ratios calculated on the basis of assumptions of −11‰ and 7‰ for the initial values of fluid and rock, respectively, prior to alteration.

https://doi.org/10.1346/CCMN.2004.0520108 Published online by Cambridge University Press

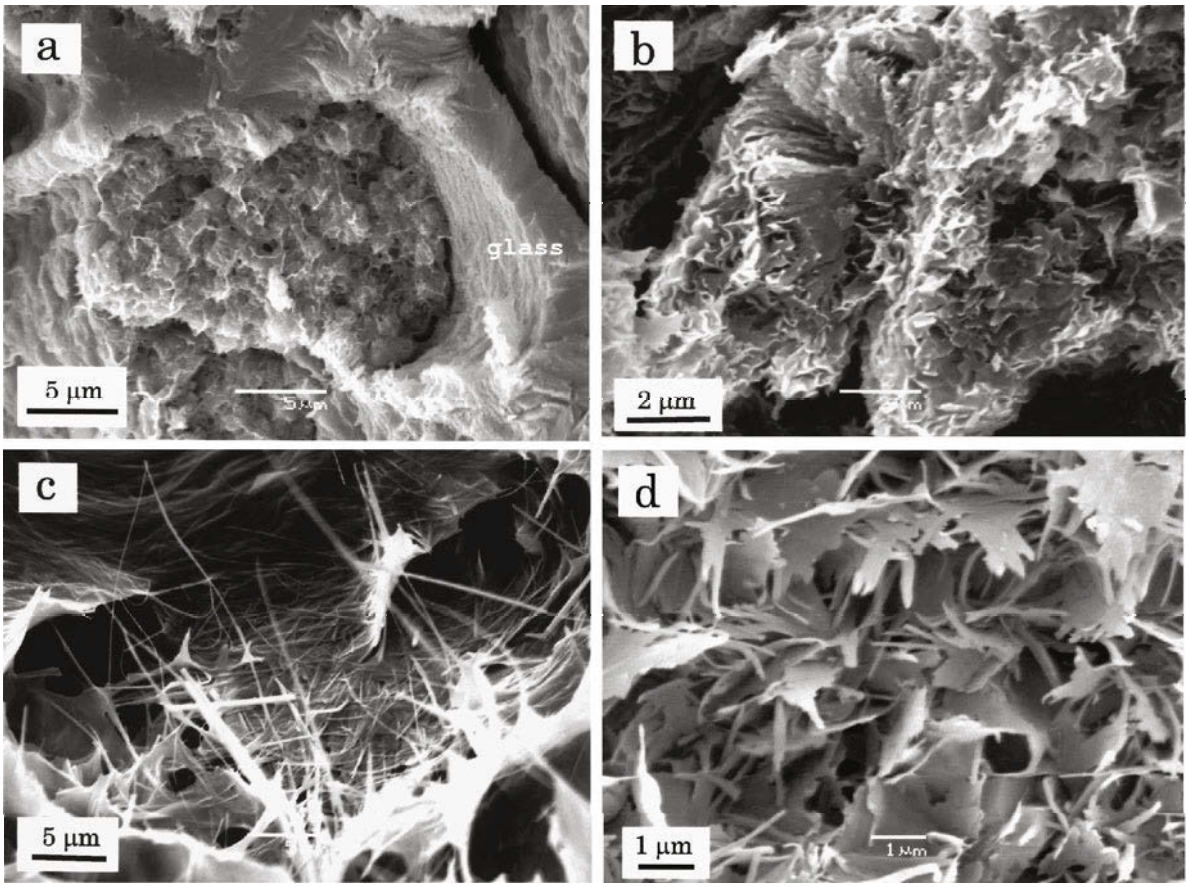

Figure 9. SEM images of alteration products: (a) montmorillonitic smectite (IT-2-320) partially replacing volcanic glass, (b) beidellitic smectite (IT-2-580) entirely replacing glass, (c) hairy I-S mineral (IT-2-664) precipitating in pore spaces in volcanics, (d) lath-shaped illite (IT-2-919).

It is known that solutions reacted with felsic vitric materials at a given temperature might increase in pH and dissolved solids, particularly Mg, Ca and Na as well as SiO_2 with increasing the degree of reaction progress. The resulting high pH and Na solution favors the formation of smectite and zeolites (*e.g.* Hay and Sheppard, 2001). In IT-2, the zeolite species changed from clinoptilolite to mordenite with increasing temperature and then the co-precipitated smectite was montmorillonite (*e.g.* 320 m and 435 m samples). As hydrolysis reaction progressed further at higher temperatures, the solution became more enriched in Na and higher in pH and favored the formation of beidellitic smectite (*e.g.* 580 m sample) and analcime, because Al in alkaline solutions is present as a tetrahedrally coordinated aluminate ion, $Al(OH)_4^-$. The abundance of aluminate ion, together with the concentrated Na ion, could promote the formation of analcime and beidellite, substituting for Si in the structures at relatively high temperatures. In the 600–740 m intervals, the hydrolytic reaction formed aluminous I-S minerals instead of beidellite by incorporating K ions into the structure from ambient solutions.

Such alteration, mentioned above, is similar to that in open hydrologic systems first described by R.L. Hay (see a recent review by Hay and Sheppard, 2001), though the present alteration occurred at higher temperatures. Unfortunately, we did not find any direct evidence of downward flow of groundwater through the drill holes. Rather, the present-day temperature profiles are almost linear (Figure 3). The exchangeable cation composition varies linearly with depth up to ~300 m as well (Figure 8). These facts suggest that although the downward migration of groundwater occurred pervasively, the flow rate may be diminished with increasing depth, so that the alteration took place approximately in a closed system. A small W/R ratio value of 0.3 obtained in the present study supports this model of crystallization process.

The mineral assemblages of altered rocks below 740 m involving dolomite, magnesite and corrensite reveal that the alteration was brought about by a saline solution, which is probably fossil seawater trapped in the Miocene formations. Previous thermodynamic calculations (Inoue *et al.*, 2001) demonstrated that the fluid recovered from IT-2 was in chemical equilibrium with

https://doi.org/10.1346/CCMN.2004.0520108 Published online by Cambridge University Press

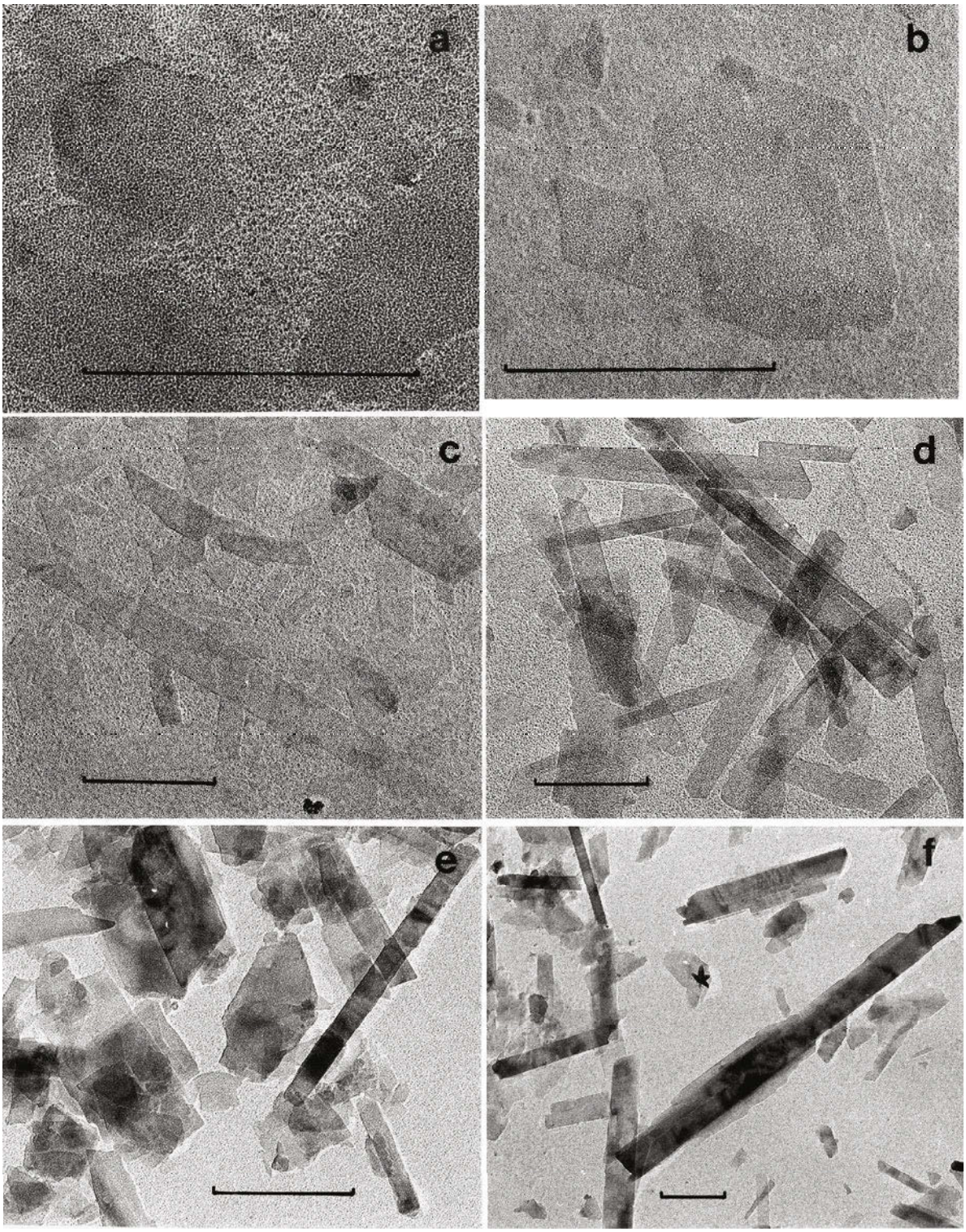

Figure 10. TEM images of I-S minerals with various %I: (a) hexagonal flake of I-S (IT-2-635, 45%I), (b) coexistence of hexagonal flake and lath (IT-2-664, 67%I), (c) thin laths (IT-2-690, 57%I), (d) thin laths (IT-2-756, 75%I), (e) mixture of thick lath and platy crystals (IT-2-873, 90%I), (f) thick laths (IT-2-919, >95%I). Scale bars are 0.5 μm.

the observed alteration minerals at *in situ* temperature. On the other hand, however, the $\delta^{18}O_{fluid}$ value calculated from the minerals did not coincide with that of the recovered fluid as noted above. When oxygen

https://doi.org/10.1346/CCMN.2004.0520108 Published online by Cambridge University Press

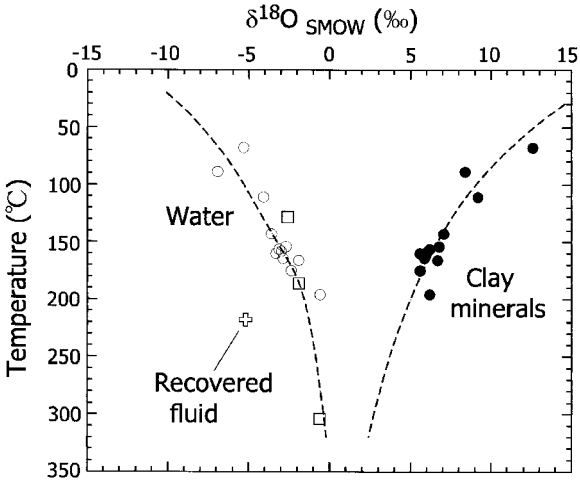

Figure 11. Variation of $\delta^{18}O$ of clay samples (solid circles) and $\delta^{18}O$ of water calculated from the data from clay samples (open circles) and carbonates (squares) assuming the equilibration between solid and fluid. The open cross symbol indicates the $\delta^{18}O$ value of hydrothermal fluid recovered at 1004 m from IT-2 after correcting the steam separation effect at recovery. The dashed curves are the simulated curves for the $\delta^{18}O$ variations of clay minerals and fluids, assuming a constant W/R mass ratio of 0.3, $\delta^{18}O_{rock} = 7‰$, and $\delta^{18}O_{fluid} = -11‰$ prior to the alteration.

fractionation during the interaction of rhyolitic to dacitic rocks with fluid was calculated approximately using the calibration curve of albite proposed by Matsuhisa *et al.* (1979), the rocks of $\delta^{18}O = 7‰$ could be equilibrated with a fluid of $\delta^{18}O_{fluid} = -0.6‰$ at 213ºC; the value is close to the *in situ* temperature (218ºC) of hydrothermal fluid recovered at 1004 m of IT-2. On the contrary, when the rock of 7‰ is in equilibrium with the recovered hydrothermal fluid of −5.2‰, the equilibrium temperature is calculated to be ~130ºC, quite distinct from the observation. Therefore, the discrepancy between the two $\delta^{18}O_{fluid}$ values suggests that the Miocene formation was not subjected to diagenesis, bringing about significant 'O-shift' in water prior to the present alteration. The observed alteration occurred at relatively earlier stages, after the deposition of Plio-Pleistocene pyroclastics, and subsequent meteoric dilution may be responsible for the observed isotopic disequilibrium.

Effect of fluid chemistry

As mentioned above, the present alteration took place under the conditions of a given rock composition and fluid/rock (W/R) ratio. Consequently the observed structural and chemical variations of clay minerals must be influenced by factors other than the effects of rock composition and W/R ratio. In order to clarify the effect of fluid chemistry on the structure and composition of I-S minerals, we compared the chemical variations of I-S minerals with those formed from similar original rocks: I-S minerals from Shinzan, Japan (Inoue and Utada, 1983) and Ponza, Italy (Ylagan *et al.*, 2000) as shown in Figure 7. Though the W/R ratios during alteration were not reported in the two systems, the chemical compositions of original rocks are not significantly different from each other. Nevertheless Figure 7 shows that the chemical compositions of clay minerals produced, especially those of intermediate I-S minerals, are different from system to system. Previous studies (Inoue *et al.*, 1987; Ylagan *et al.*, 2000) attributed the entire smectite-to-illite reaction to the dissolution and crystallization (DC) processes. This DC model is, strictly speaking, different from the present dissolution-precipitation model. For instance, Inoue *et al.* (1987) interpreted the conversion from smectite to R1 I-S minerals (<50%I) to be responsible for the K fixation by precursor smectite due to the slight increase in layer charge. Since the continuous R0-to-R1 conversion was not recognized in the present study, we cannot discuss the detailed fluid chemistry effect on the chemical composition of R0 I-S minerals. Comparing the chemical compositions of R1 I-S minerals which were regarded as newly precipitated phases in either the DC or the present model, it suggests that the chemical composition of clay minerals precipitated *in situ* is a function of the fluid chemistry participating in the alteration reaction. According to previous studies, the reacting solutions in the Shinzan and Ponza systems both were significantly concerned with seawater. Thus, the precipitation of aluminous smectite and I-S minerals observed in the range of ~580 to 740 m in IT-2 was caused by high pH and Na-rich solutions derived from reaction of felsic glass with groundwater. Ylagan *et al.* (2000) noted that the formation of relatively Mg-rich I-S minerals in Ponza was related to the contribution of seawater. This is exemplified more clearly by the present observations in which I-S and illitic minerals precipitated below 740 m become enriched in Mg.

Ostwald step rule behavior of I-S mineral crystallization

As shown in Figure 6, the observed relationship between temperature (T) and %I in I-S minerals is characteristic, as is the variation in chemical composition. The maximum temperature (~220–250ºC) of the appearance of I-S minerals is almost equivalent to those reported previously from other hydrothermal systems (*e.g.* Inoue, 1995; Ylagan *et al.*, 2000). Smectite precipitates up to ~150ºC and with slight increase in temperature, the precipitation of R1 ordered I-S minerals follows without the continuous precipitation of intermediate R0 I-S minerals. It is also characteristic that more than two types of I-S minerals coexist at intermediate stages. The high maximum temperature (~150ºC) for smectite relative to those in burial diagenesis is in part attributed to the composition of precipitating smectite, taking account of many experimental observations that aluminous smectite exists up to relatively higher temperatures than the Mg variety (*e.g.* Velde, 1985).

https://doi.org/10.1346/CCMN.2004.0520108 Published online by Cambridge University Press

On the other hand, Essene and Peacor (1995) pointed out that most I-S minerals, even the end-member smectite and illite, are thermodynamically metastable and the sequential reactions from smectite to illite through I-S minerals should be understood with kinetic concepts based on the Ostwald step rule. As a matter of course, the *T vs.* %I relation mentioned above must be explained from the viewpoint of the Ostwald step rule. For it, we assume here hypothetical logarithmic solubility product (K_{sp}) curves of smectite and R1 I-S mineral with a specific structure, composition, and size as a function of temperature in the system K_2O-Na_2O-Al_2O_3-SiO_2-H_2O, as well as that of illite. Smectite has a different composition and is generally a favored phase at lower temperatures than the R1 I-S mineral. The facts predict reasonably that the two solubility product curves intersect at a temperature T_c as shown in Figure 12a.

There are many factors related to Ostwald step rule behavior, but it is primarily important to consider the relative nucleation rates of solid phases being formed at a given temperature (Morse and Casey, 1988). Unfortunately there is a lack of knowledge about the geometrical factor of crystal nuclei, the surface energy, and the molar volume of clay minerals in relation to the nucleation rates. Despite that, Ostwald step rule behavior will operate when crystallization takes place below and near the intersection temperature (*e.g.* T_c of Figure 12a) and/or at very high supersaturations (Mutaftschiev, 2001). When the composition of supersaturated fluid is represented by point A at temperature T_1 or A′ at T_2 of Figure 12a, the supersaturations with respect to smectite and I-S mineral can be defined by the length AC and AB at temperature T_1 and by the length A′C′ and A′B′ at T_2, respectively. At T_2 near T_c, for instance, the crystallization will take place through the first precipitation of R1 I-S mineral as a metastable phase relative to smectite because the difference between the supersaturations with respect to smectite (length A′C′) and R1 I-S (length A′B′) becomes too small to compensate for the effects of geometrical factor, surface energy and molar volume of two minerals (Mutaftschiev, 2001). Besides the effect of nucleation rate, the extent of thermal gradient prevailing in the study area can be related to the period of time when the system can attain the threshold temperature, *i.e.* T_c. The above virtual analysis leads to the mode of occurrence of precipitated clay minerals as schematically illustrated in Figure 12b, which is similar to the present observations. In summary, the relationship of *T vs.* %I (Figure 6) can be interpreted on the assumption that the transformation of smectite to R1 ordered structure occurred abruptly under high thermal gradient (*e.g.* ~15–20ºC/100 m) with few intermediate R0 structures, was subject to the Ostwald step rule, and that the boundary temperature of smectite and R1 structure increased under the chemical conditions favorable to the precipitation of aluminous clay minerals.

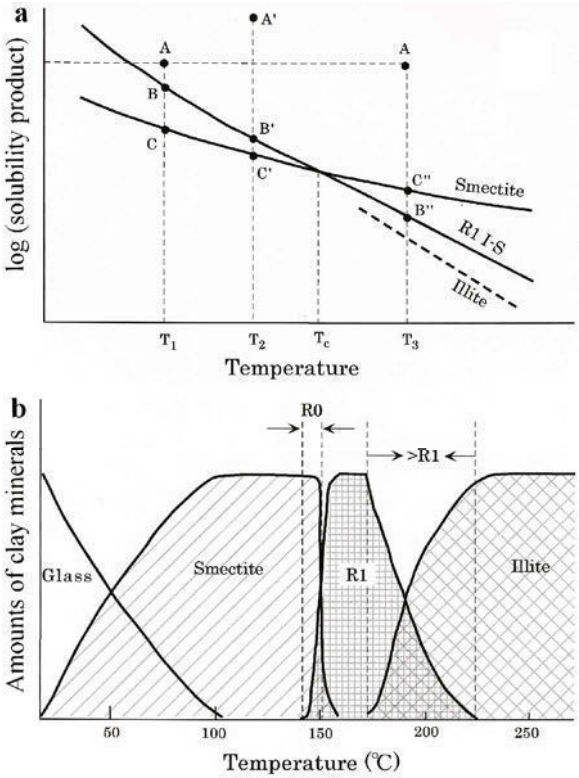

Figure 12. (a) Hypothetical relationship between logarithmic solubility product curves of smectite, R1 I-S mineral, and illite as a function of temperature. (b) Conceptual model illustrating the relationship between temperature and amounts of clays precipitated *in situ*.

Moreover, it can be emphasized from Figure 12 that the R1 ordered I-S mineral may be a unique phase and intermediate R0 I-S minerals are mixed-phases of smectite and R1 with various proportions. Altaner *et al.* (1988) indicated in their ^{29}Si NMR measurements that R1 ordered I-S minerals like rectorite have a structure consisting of polar 2:1 layers where the interstratification is interlayer centered, and each layer is identical but contains two low-charge and high-charge tetrahedral sheets. Stixrude and Peacor (2002) demonstrated that the polar 2:1 layer structure has a total energy lower than the non-polar structure for R1 ordered I-S minerals on the basis of first-principles quantum mechanical calculation. Also, recent high-resolution transmission electron microscopy studies of I-S minerals (*e.g.* Dong *et al.*, 1997; Tillick *et al.*, 2001; Yan *et al.*, 2001; Bauluz *et al.*, 2002) provide many observations which support the above conclusion.

The transformation of R1 to illite including >R1 structures may also be described by a mixed-phase system of R1 and illite under the control of the Ostwald step rule, although the *T vs.* %I relation seems to be apparently continuous (Figure 6). However, the solubility product curve of illite may not be so different from that of R1 I-S as shown in Figure 12a. The precipitated crystals basically contain a mica layer unit and they will

https://doi.org/10.1346/CCMN.2004.0520108 Published online by Cambridge University Press

undergo the successive crystal growth process under the conditions where precipitation occurred. As a result, the reaction progress of R1-to-illite can be represented by the extent of crystal growth, as noted by many previous works (Inoue *et al.*, 1987, 1988; Inoue and Kitagawa, 1994; Ylagan *et al.*, 2000).

SUMMARY AND CONCLUSIONS

The present study provides information about how I-S minerals crystallize under given conditions such as negligible time effect, high geothermal gradient, a given composition of precursor materials, and constant fluid/rock ratio during the formation of clay minerals. The observed textural relationships of product clay minerals indicated that all the I-S minerals formed simultaneously via direct precipitation from solution at different temperatures rather than through a series of sequential transformation reactions from precursor smectite. This conclusion confirms the previous hypothesis proposed by Bethke *et al.* (1986). Based upon the model proposed in the present study, the fluid chemistry affects primarily the chemical composition and as a result, the structure of I-S minerals *in situ* precipitated at respective temperatures. An aluminous R1 ordered I-S mineral precipitates as a unique phase at relatively higher temperatures and intermediate R0 minerals may be a mixed phase of smectite and R1 which appeared as a result of the Ostwald step rule behavior in smectite illitization processes.

Although, indeed, all the I-S series minerals may be thermodynamically metastable phases (Essene and Peacor, 1995), *in situ* precipitation of I-S minerals might take place in chemical and isotopic equilibrium with the reacting solution. Thus, examining both the interstratification mineralogy and oxygen isotope composition of I-S minerals is useful for reconstructing the thermal and geochemical histories as well as paleohydrology during alteration in active and extinct hydrothermal systems.

ACKNOWLEDGMENTS

A. Inoue is grateful to CNRS, France, for providing an opportunity to stay in Poitiers University to collaborate on this work. The authors are also grateful to Bruce Velde (ENS) and Bruno Lanson (J. Fourier University) for stimulating discussion in the course of completing this study. This work would not have been possible without the help of Junko Hara (Tohoku University) and Akira Imai (University of Tokyo) in the XRD work on core samples, and in the measurement of homogenization temperature of fluid inclusions, and isotope values of carbonates. Reviews by E.J. Essene, B. Bauluz and C. Elliott helped to improve the manuscript.

REFERENCES

Altaner, S.P. and Ylagan, R.F. (1997) Comparison of structural models of mixed-layer illite/smectite and reaction mechanisms of smectite illitization. *Clays and Clay Minerals*, **45**, 517–533.

Altaner, S.P., Weiss, C.A. and Kirkpatrick, R.J. (1988) Evidence from ^{29}Si NMR for the structure of mixed-layer illite/smectite clay minerals. *Nature*, **331**, 699–702.

Bailey, S. W. (1980) Structures of layer silicates. Pp. 2–123 in: *Crystal Structures of Clay Minerals and their X-ray Identification* (G.W. Brindley and G. Brown, editors). Monograph **5**, Mineralogical Society, London.

Bauluz, B., Peacor, D.R. and Ylagan, R.T. (2002) Transmission electron microscopy study of smectite illitization during hydrothermal alteration of a rhyolitic hyaloclastite from Ponza, Italy. *Clays and Clay Minerals*, **50**, 157–173.

Bethke, C.M., Vergo, N. and Altaner, S.P. (1986) Pathways of smectite illitization. *Clays and Clay Minerals*, **34**, 125–135.

Bish, D.L. and Aronson, J.L. (1993) Paleogeothermal and paleohydrologic conditions in silicic tuff from Yucca Mountain, Nevada. *Clays and Clay Minerals*, **41**, 148–161.

Christidis, G.E. (1998) Comparative study of the mobility of major and trace elements during alteration of an andesite and a rhyolite to bentonite, in the islands of Milos and Kimolos, Aegean Sea, Greece. *Clays and Clay Minerals*, **46**, 379–399.

Clayton, R.N. and Mayeda, T.K. (1963) The use of bromine pentafluoride in the extraction of oxygen from oxides and silicates for isotope analysis. *Geochimica et Cosmochimica Acta*, **27**, 43–52.

Dong, H., Peacor, D.R. and Freed, R.L. (1997) Phase relations among smectite, R1 illite-smectite, and illite. *American Mineralogist*, **82**, 379–391.

Essene, E.J. and Peacor, D.R. (1995) Clay mineral thermometry – A critical perspective. *Clays and Clay Minerals*, **43**, 540–553.

Hay, R.L. and Sheppard, R.A. (2001) Occurrence of zeolites in sedimentary rocks: An overview. Pp. 217–234 in: *Natural Zeolites: Occurrence, Properties, Applications* (D.L. Bish and D.W. Ming, editors). Reviews in Mineralogy and Geochemistry, **45**. Mineralogical Society of America, Washington, D.C.

Inoue, A. (1995) Formation of clay minerals in hydrothermal environments. Pp. 268–329 in: *Origin and Mineralogy of Clays* (B. Velde, editor), Springer, Berlin.

Inoue, A. (2000) Two-dimensional variations of exchangeable cation composition in the terrigenous sediment, eastern flank of the Juan de Fuca Ridge. *Marine Geology*, **162**, 501–528.

Inoue, A. and Kitagawa, R. (1994) Morphological characteristics of illitic clay minerals from a hydrothermal system. *American Mineralogist*, **79**, 700–711.

Inoue, A. and Utada, M. (1983) Further investigations of a conversion series of dioctahedral mica/smectites in the Shinzan hydrothermal alteration area, northeast Japan. *Clays and Clay Minerals*, **31**, 401–412.

Inoue, A., Kohyama, N., Kitagawa, R. and Watanabe, T. (1987) Chemical and morphological evidence for the conversion of smectite to illite. *Clays and Clay Minerals*, **35**, 111–120.

Inoue, A., Velde, B., Meunier, A. and Touchard, G. (1988) Mechanism of illite formation during smectite-to-illite conversion in a hydrothermal system. *American Mineralogist*, **73**, 1325–1334.

Inoue, A., Bouchet, A., Velde, B. and Meunier, A. (1989) Convenient technique for estimating smectite layer percentage in randomly interstratified illite/smectite minerals. *Clays and Clay Minerals*, **37**, 227–234.

Inoue, A., Hara, J. and Imai, A. (2001) Genesis of Na-series rock alteration widespread in the southeastern area of Hachimantai geothermal field: water-rock interactions

driven by descending groundwater and fossil seawater. *Shigen-Chishitsu (Journal of Society of Resource Geology Japan)*, **51**, 101–120 (in Japanese).

Kanisawa, S., Doi, N., Kato, O. and Ishikawa, K. (1994) Quaternary Kakkonda Granite underlying the Kakkonda geothermal field, Northeast Japan. *Journal of Mineralogy, Petrology and Economic Geology*, **89**, 390–407 (in Japanese).

Kato, O. and Sato, K. (1995) Development of deep-seated geothermal reservoir bringing the Quaternary granite into focus in the Kakkonda geothermal field. *Shigen-Chishitsu* (*Journal of Society of Resource Geology Japan*), **45**, 131–144 (in Japanese).

Larson, P.B. and Taylor, H.P. (1986) An oxygen isotope study of hydrothermal alteration in the Lake City Caldera, San Juan Mountain, Colorado. *Journal of Volcanology and Geothermal Research*, **30**, 47–82.

Matsuhisa, Y. (1979) Oxygen isotopic compositions of volcanic rocks from the east Japan island arcs and their bearing on petrogenesis. *Journal of Volcanology and Geothermal Research*, **5**, 271–296.

Matsuhisa, Y., Goldsmith, J.R. and Clayton, R.N. (1979) Oxygen isotopic fractionation in the system quartz-albite-anorthite-water. *Geochimica et Cosmochimica Acta*, **43**, 1131–1140.

Morse, J.W. and Casey, W.H. (1988) Ostwald processes and mineral paragenesis in sediments. *American Journal of Science*, **288**, 537–560.

Muraoka, H., Uchida, T., Sasada, M., Yagi, M., Akaku, K., Sasaki, M., Yasukawa, K., Miyazaki, S., Doi, N., Saito, S., Sato, K. and Tanaka, S. (1998) Deep geothermal resources survey program: Igneous, metamorphic and hydrothermal processes in a well encountering 500ºC at 3729 m depth, Kakkonda, Japan. *Geothermics*, **27**, 507–534.

Mutaftschiev, B. (2001) *The Atomistic Nature of Crystal Growth*. Springer, Berlin, 368 pp.

Nakamura, H. and Sumi, K. (1981) Exploration and development at Takinoue, Japan. Pp. 247–272 in: *Geothermal Systems: Principles and Case Histories* (L. Rybach and L.J.P. Muffler, editors), John Wiley & Sons, Chichester, UK.

NEDO (1993) Western area of Mt. Iwate. *Report of Investigations for Geothermal Exploration and Development*, **31**, 1289 pp. (in Japanese).

Patrier, P., Papapanagiotou, P., Beaufort, D., Traineau, H., Bril, H. and Rojas, J. (1998) Role of permeability versus. temperature in the distribution of the fine (<0.2 μm) clay fraction in the Chipilapa geothermal system (El Salvador, Central America). *Journal of Volcanology and Geothermal Research*, **72**, 101–120.

Reynolds, R.C., Jr. (1985) *NEWMOD© : A computer program for the calculation of one-dimensional diffraction patterns of mixed-layered clays*. R.C. Reynolds, 8 Brook Rd., Hanover, New Hampshire, USA.

Savin, S.M. and Lee, M. (1988) Isotopic studies of phyllosilicates. Pp. 189-223 in: *Hydrous Phyllosilicates* (S.W. Bailey, editor). Reviews in Mineralogy, **19**. Mineralogical Society of America, Washington, D.C.

Stixrude, L. and Peacor, D.R. (2002) First-principles study of illite-smectite and implications for clay mineral systems. *Nature*, **420**, 165–168.

Taylor, H.P., Jr. (1974) The application of oxygen and hydrogen isotope studies to problems of hydrothermal alteration and ore deposition. *Economic Geology*, **69**, 843–883.

Thompson, A.B. (1971) Analcime-albite equilibria at low temperatures. *American Journal of Science*, **271**, 79–92.

Tillick, D.A., Peacor, D.R. and Mauk, J.L. (2001) Genesis of dioctahedral phyllosilicates during hydrothermal alteration of volcanic rocks: I. The Golden Cross epithermal ore deposit, New Zealand. *Clays and Clay Minerals*, **49**, 126–140.

Velde, B. (1985) *Clay Minerals: A Physico-Chemical Explanation of their Occurrence*. Elsevier, Amsterdam, 427 pp.

Watanabe, T. (1981) Identification of illite/montmorillonite interstratifications by X-ray powder diffraction. *Journal of Mineralogical Society Japan, Special Issue*, **15**, 32–41 (in Japanese).

White, A.F., Chuma, N.J. and Goff, F. (1992) Mass transfer constraints on the chemical evolution of an active hydrothermal system, Valles Caldera, New Mexico. *Journal of Volcanology and Geothermal Research*, **49**, 233–253.

Yan, Y., Tillick, D.A., Peacor, D.R. and Simmons, S.F. (2001) Genesis of dioctahedral phyllosilicates during hydrothermal alteration of volcanic rocks: II. The Broadlands-Ohaaki hydrothermal system, New Zealand. *Clays and Clay Minerals*, **49**, 141–155.

Ylagan, R.F., Altaner, S.P. and Pozzuoli, A.P. (2000) Reaction mechanisms of smectite illitization associated with hydrothermal alteration from Ponza island, Italy. *Clays and Clay Minerals*, **48**, 610–631.

(*Received 12 November 2002; revised 12 August 2003; Ms. 738; A.E. W. Crawford Elliott*)

APPENDIX

In a closed system, the isotopic mass-balance before and after the alteration reaction may be written as follows:

$$m_i\delta^{18}O_i^w + n_i\delta^{18}O_i^r = m_f\delta^{18}O_f^w + \Sigma n_f\delta^{18}O_f^p \quad (A1)$$

and

$$m_i + n_i = m_f + \Sigma n_f \quad (A2)$$

where m and n denote the moles of oxygen in fluid and solid phases and subscripts i and f stand for the initial and final states of the system, respectively. $\delta^{18}O_i^w$ and $\delta^{18}O_i^r$ are the oxygen isotope ratios of fluid and rock prior to alteration, and $\delta^{18}O_f^p$ are those of secondary minerals formed by the alteration, respectively. If product mineral phases are in equilibrium with a fluid at a given temperature, the isotope ratio of each phase can be written by:

$$\delta^{18}O_f^p = \delta^{18}O_f^w + \Delta_{p\text{-}w} \quad (A3)$$

Putting equations A2 and A3 into equation A1, the fluid/rock (W/R) ratio is:

$$W/R = m_i/n_i = [\delta^{18}O_i^r - \delta^{18}O_f^w - \Sigma(n_f/n_i)\cdot\Delta_{p\text{-}w}]/(\delta^{18}O_f^w - \delta^{18}O_i^w) \quad (A4)$$

Using equation A4 and assuming appropriate values of $\delta^{18}O_i^r$ and $\delta^{18}O_i^w$, we can calculate a W/R ratio during the formation of I-S minerals at a given temperature.

Here we used a dissolution-precipitation model for clay mineral formation in order to evaluate W/R ratio. In

the dissolution-precipitation model, the reactant glass is out of isotopic equilibrium with the product mineral-fluid system. Thus the dissolution results in unequal addition of oxygen isotope to the mass balance of the system. Subsequently formed product minerals precipitate in isotopic equilibrium with the fluid. If the reactant rhyolite to dacite glass is represented approximately by an albite composition, the formation of clay minerals can be written by the following Al-conservative reaction, for smectite ($Na_{0.33}Al_{2.33}Si_{3.67}O_{10}(OH)_2$),

$$NaAlSi_3O_8 + 0.858H^+ = 0.429Na_{0.33}Al_{2.33}Si_{3.67}O_{10}(OH)_2 + 0.858Na^+ + 1.425SiO_2(aq) \quad (A5)$$

and for illite ($K_{0.9}Al_{2.90}Si_{3.10}O_{10}(OH)_2$),

$$NaAlSi_3O_8 + 0.31K^+ + 0.69H^+ = 0.345K_{0.9}Al_{2.90}Si_{3.10}O_{10}(OH)_2 + Na^+ + 1.931SiO_2(aq) \quad (A6)$$

In equations A5 and A6, dissolving 1 mole of albite glass forms 0.429 moles of beidellite and 0.345 moles of illite, respectively. In terms of oxygen exchange, these values correspond to 0.6435 (= 0.429 × [12/8]) and 0.126 (= 0.345 × [12/8]), respectively. Consequently, the term n_f/n_i of equation A4 becomes $\{0.429 \times (12/8) \times (1 - I) + 0.345 \times (12/8) \times I\}$ as a function of the fractional content of illite layer (I). Finally, we obtain an equation describing the change in W/R ratio with increase in illite layer, using equation 1 in the text:

$$W/R = [\delta^{18}O_i^r - \delta^{18}O_f^w - (0.6435 - 0.126I)\Delta_{I/S\text{-}w}]/(\delta^{18}O_f^w - \delta^{18}O_i^w) \quad (A7)$$

Here, we took into consideration only the isotopic exchange reaction of structural sites in smectite and illite because the interlayer water is able to exchange more easily with the surrounding fluid and thus the isotope ratios are approximately equal to those of the fluid phase. Also, we ignored the effects of co-precipitating minerals such as silica polymorphs, zeolites and carbonates for simplicity. The W/R of the above equations is the atomic ratio. The atomic ratio can easily be converted to the mass ratio by multiplying by 0.55 because the wt.% oxygen is 88.8% in water and 48.8% in rock (albite).

https://doi.org/10.1346/CCMN.2004.0520108 Published online by Cambridge University Press